論文 / 著書情報
Article / Book Information

Title	Strength and Behavior of Elastic Critical Distortional Buckling for Cold - Formed Channel Member Under Compression
Authors	Kazuya Mitsui, Kikuo Ikarashi, Tomoki Kobashi, Ryohei Kuwada
Citation	Japan Architectural Review, Vol. 8, Issue 1, e70024
Pub. date	2025, 5
DOI	https://doi.org/10.1002/2475-8876.70024
Creative Commons	Information is in the article.

TRANSLATED PAPER OPEN ACCESS

Strength and Behavior of Elastic Critical Distortional Buckling for Cold-Formed Channel Member Under Compression

Kazuya Mitsui[1] | Kikuo Ikarashi[1] | Tomoki Kobashi[2] | Ryohei Kuwada[3]

[1]Department of Architecture and Building Engineering, Institute of Science Tokyo, Tokyo, Japan | [2]Department of Architecture, Chiba Institute of Technology, Chiba, Japan | [3]Steel Research Lab, Nippon Steel Corporation, Chiba, Japan

Correspondence: Kazuya Mitsui (mitsui.k.ad@m.titech.ac.jp)

Received: 1 December 2024 | **Revised:** 25 March 2025 | **Accepted:** 24 April 2025

Funding: This work was supported by Japan Society for the Promotion of Science (Grant JP20H02294).

Keywords: channel member | distortional buckling | energy method | thin-walled steel structures

ABSTRACT

Distortional buckling of channel members is a critical factor in steel structures composed of thin-walled members; however, existing models have limitations in accurately predicting this behavior. This study analyzes the distortional buckling behavior of channel members using an energy method. A nonconventional mechanical model and displacement functions are introduced to simulate distortional buckling behavior, highlighting the limitations of conventional models. An evaluation formula for the elastic distortional buckling strength is derived, directly reflecting the geometrical parameters of the channel member using the proposed mechanical model. Additionally, a design equation is formulated. The proposed evaluation formula and simplified design equation enable the precise determination of the elastic critical distortional buckling strength, including cases where distortional buckling is initiated by local buckling of the web, which previous evaluation formulas could not address. These methods enable continuous evaluation of distortional buckling in channel members. The proposed formula and design equation were verified against finite element analysis results, confirming their reliability and effectiveness. The developed model and equations offer improved accuracy over conventional approaches for predicting distortional buckling in channel members, demonstrating their reliability and applicability under diverse conditions.

1 | Introduction

When a compressive force is applied axially to a uniaxially symmetric open-section member, such as a cold-formed lipped channel member or channel member (hereinafter collectively referred to as a "channel member"), four types of buckling may occur: (A) distortional, (B) local, (C) flexural, and (D) flexural-torsional buckling (Figure 1). Distortional and local buckling are characterized by deformation within the cross-section (local system), whereas flexural and flexural-torsional buckling involve the global system behavior without cross-sectional deformation. In channel members under compressive forces, buckling may occur individually in combination with these modes [1–3]. International research has focused on distortional buckling, with significant contributions from Hancock et al. [3–6] and Schafer et al. [7–10] Hancock et al.

The Japanese version of this paper was published in Volume 87 Number 791, pages 139–148, https://doi.org/10.3130/aijs.87.139 of *Journal of Structural and Construction Engineering* (*Transactions of AIJ*). The authors have obtained permission for secondary publication of the English version in another journal from the Editor of *Journal of Structural and Construction Engineering* (*Transactions of AIJ*). This paper is based on the translation of the Japanese version with some slight modifications.

[3, 4] regarded distortional buckling as local buckling of the flange and proposed a mechanical model (see Figure 2A) to derive a formula for elastic critical distortional buckling. In this model, two types of elastic springs at the flange-web junction accounted for the web's restraining effect on the flange. The buckling strength was derived from the balance of the forces. Hancock et al. [5, 6] also presented a buckling strength curve for distortional buckling based on the effective width theory developed by Winter [11] for local buckling and a post-buckling strength curve using Johnston's buckling strength curve [12] Schafer et al. [7] found that the formula for the distortional buckling strength in the American Iron and Steel Institute (AISI) design [13] was overly conservative. They proposed a novel mechanical model with three types of elastic springs placed at the flange-to-web junction line (Figure 2B), similar to the model proposed by Hancock. Furthermore, a formula for the post-buckling strength was derived from the elastic critical distortional buckling strength, demonstrating that the experimental results could be accurately assessed. Studies on distortional buckling have also been conducted in Japan. Iwamoto et al. [14] explored the relationship between geometrical properties, such as lip width and length-to-flange width ratio, and qualitatively clarified the elastic critical distortional buckling strength using a model with a simply supported flange-to-web junction line through a finite element method (FEM).

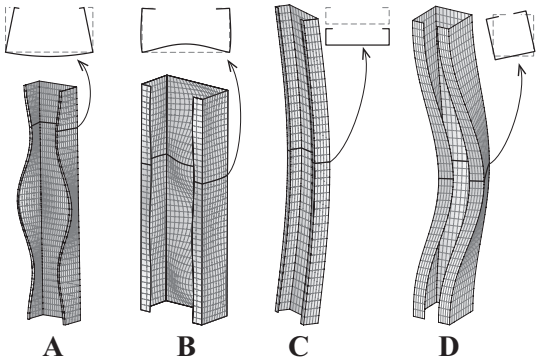

FIGURE 1 | Buckling modes in the channel member. (A) Distortion. (B) Local. (C) Flexural. (D) Flexural-torsional.

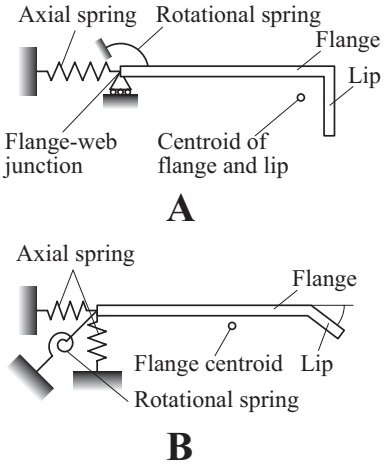

FIGURE 2 | Mechanical models for the distortional buckling mode. (A) Hancock model. (B) The Schafer model.

In the aforementioned study [3, 4, 7], the buckling behavior of elastic distortional buckling was modeled as the local buckling of a flange, with one side supported being simply supported, elastically supported, or clamped, while the other end is free, as shown in Figure 2. The restraining effect of the web on the flange is represented by elastic springs, which indirectly represent this effect; however, it remains unclear whether this approximation is appropriate. Additionally, the restraining effect of the flange on the web was not considered. Therefore, this study proposes a new evaluation formula for the elastic critical distortional buckling strength of channel members, explicitly incorporating member geometry through the energy method. This approach incorporates the interactions between each plate element within a mechanical model by representing the web, flange, and lip-buckling waveforms as displacement functions. Subsequently, the relationship between cross-sectional geometry and distortional buckling behavior in channel members is numerically analyzed using the proposed formula. Finally, a design equation is formulated by simplifying the proposed evaluation formula, and its validity is assessed through comparison with FEM results.

This study focuses on the cross-sectional geometry and distortional buckling behavior of channel members without intermediate stiffeners on the web and flange, as shown in Figures 3

Cross-sectional Deflection	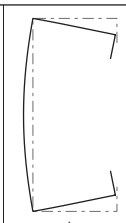 A	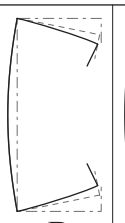 B	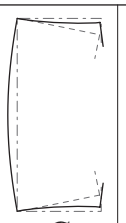 C	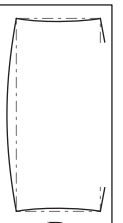 D
Buckling mode	Pure distortional	Distortional	Coupled	Local
Out-of-plane deformation of flanges	Keep straight	Bend away from junction	Bend approaching junction	Bend approaching junction
Transfer of the flange-lip junctions/ web-flange junctions	Positive/ Negative	Positive/ Negative	Positive/ Negative	Negative/ Negative

FIGURE 3 | Definition of buckling modes. (A) Pure distortion. (B) Distortion. (C) Coupled. (D) Local buckling.

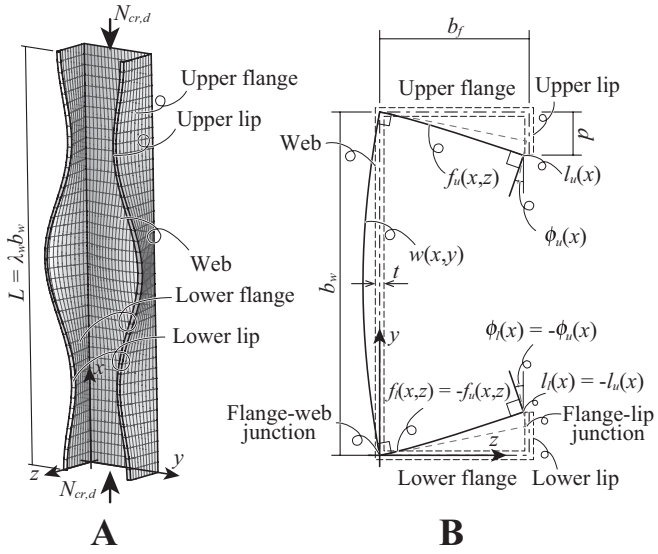

FIGURE 4 | Distortional buckling under uniform compression. (A) Buckling deformation. (B) Cross-sectional deformation.

and 4. Each plate element is connected orthogonally, and neither other buckling modes nor coupled buckling effects are considered. The buckling behavior of the local system in the channel member under uniform compressive stress is shown in Figure 3. Previous studies have provided ambiguous definitions of distortional buckling deformation; however, a commonly observed characteristic was the movement of the junction line between the flange and lip. The authors considered this classification to be not entirely accurate, as it involved coupled buckling with local buckling, as shown in Figure 3C. Therefore, in this study, pure distortional buckling is defined as a buckling mode in which the junction line between the web and flange remains stationary, while the junction line between the flange and lip moves (Figure 3A). In this scenario, the flanges rotate around the junction line between the web and flanges, and the flange plate elements maintain a straight line. Furthermore, when the junction line between the flange and lip moves, the buckling mode where the flange bends away from the junction line (Figure 3B) is defined as distortional buckling. Conversely, the buckling mode in which the flange bends toward the junction line of the flange and lip (Figure 3C) is classified as coupled buckling with local buckling. This study considers only pure distortional buckling (Figure 3A) and distortional buckling (Figure 3B). Hereafter, both buckling modes are collectively referred to as distortional buckling. Notably, local buckling refers to a buckling mode in which the junction lines of each plate element remain stationary (Figure 3D) [15–17].

2 | Derivation of the Elastic Critical Distortional Buckling Strength Formula for Cold-Formed Channel Members

2.1 | Mechanical Model for Distortional Buckling and Buckling Displacement Functions

Figure 4 illustrates the mechanical model corresponding to the deformation caused by distortional buckling. In this model, b_w is the web depth, b_f is the flange width, d is the lip width, t is the thickness, L is the member length, and $\lambda_w \left(= L / b_w\right)$ is the aspect ratio of the web. The cross-sectional plate thickness was uniform and concentrated along the section's centerline, with the corner bends of the cross-section neglected. Table 1 summarizes the variables used to describe the cross-sectional shapes and stress states of channel members. In the mechanical model, rotation was restrained at both ends of the member, preventing global buckling such as flexural buckling. However, rotation about the width axis of each plate element was allowed. During distortional buckling, the displacement within the cross-section at any location is characterized by no movement along the flange-web junction, while adjacent plate elements remain orthogonal. By defining displacement functions that satisfy these deformation conditions, the buckling displacements of the web, flange, and lip can be continuously represented, capturing the plate-element interaction in the buckling strength formula. The displacement function for the upper flange, $f_u(x,z)$, is initially defined. The displacement within the flange cross-section involves rotation about the flange-web junction and out-of-plane flexural deformation of the plate element, which is approximated by the following function:

$$f_u(x,z) = \mu_k(x)\left[d_a \frac{z}{b_f} + d_b\left(1 - \cos\frac{\pi z}{2b_f}\right)\right] \quad (1)$$

TABLE 1 | Parameters and symbols.

E	Young's modulus [N/mm^2] (=205000)	D	Flexural rigidity of plane [Nmm]
G	Shear modulus [N/mm^2] (= E/(2 (1 + ν))		(= Et^3/(12 (1-ν^2)))
ν	Poisson's ratio [−] (=0.3)	A_g	Gross area [mm^2]
b_w	Web depth [mm]	A_l	Area of a lip [mm^2]
b_f	Flange width [mm]	I_l	Moment of inertia of a lip [mm^4]
d	Lip width [mm]	J_l	Torsion constant of a lip [mm^3]
t	Thickness [mm]	$N_{cr,d}$	Elastic critical distortional buckling strength [N]
L	Member length [mm]	$\sigma_{cr,d}$	Elastic critical distortional buckling stress [N/mm^2]
λ_w	Web aspect ratio [−] (= L/b_w)	l_{cr}	Buckling half-wavelength [mm]
$k_{w,d}$	Buckling coefficient of the web determined by distortional buckling [−] (= $\sigma_{cr,d}$12 (1-ν^2) $b_w{}^2/(\pi^2 Et^2)$)	$k_{f,d}$	Buckling coefficient of the flange determined by distortional buckling [−] (= $\sigma_{cr,d}$ 12 (1 − ν^2) $b_f{}^2/(\pi^2 Et^2)$)

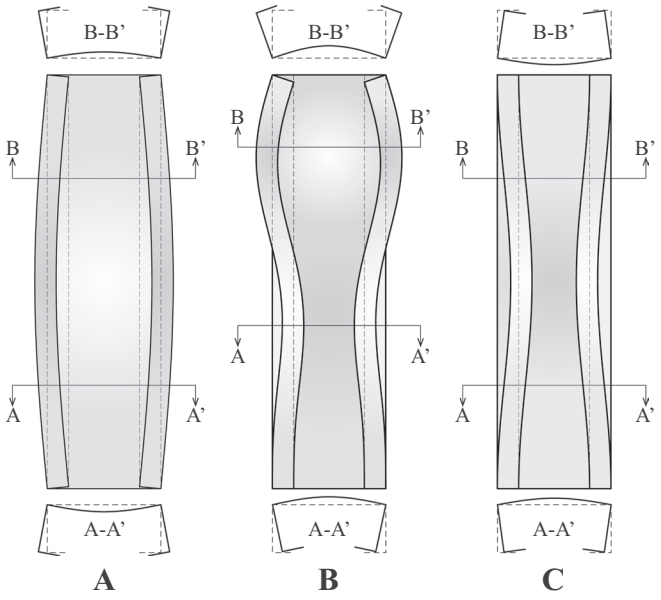

FIGURE 5 | Distortional buckling deformation in the longitudinal direction. (A) Pinned-pinned support, as shown in Equation (6A). (B) The pinned-clamped support shown in Equation (6B). (C) Clamped–clamped support shown in Equation (6C).

The first term within the parentheses on the right side of Equation (1) approximates the buckling deformation of the flange when it buckles under a simply supported boundary condition at the flange-web junction line. Conversely, the second term represents the buckling deformation when the junction line is clamped [18] Parameters d_a and d_b are coefficients that determine the buckling displacement within the cross-section. Only one side of the flange and lip is considered due to the axial symmetry of the buckling deformation. The function $\mu_k(x)$ represents the buckling deformation along the longitudinal direction (x-axis) and will be discussed in detail later. By setting $d_b = 0$, the out-of-plane flexural deformation of the flange is eliminated, allowing the pure distortional buckling deformation of the flange to be represented, as illustrated in Figure 3A. As the flange-web junction is stationary, the displacement function of the web, $w(x,y)$, can be expressed as:

$$w(x,y) = \mu_k(x) d_b \sin\frac{\pi y}{b_w}, \tag{2}$$

where d_c is an undetermined coefficient. As the flanges and web remain orthogonal along their junction lines, the displacement functions of the flange and web satisfy the following relationship:

$$\left.\frac{\partial f_u(x,z)}{\partial z}\right|_{z=0} = \left.\frac{\partial w(x,y)}{\partial y}\right|_{y=b_w} \tag{3}$$

The in-plane deformation of the upper lip, $l_u(x)$, matches the deformation at the flange tip, as expressed in Equation (4). Similarly, due to the orthogonality condition with the flange, the rotation of upper lip, $\phi_u(x)$, matches the rotation at the flange tip and can be expressed by the function shown in Equation (5). However, because the lip width is relatively small compared with those of the web and flange, its out-of-plane flexural deformation can be neglected. For simplicity, the lip was treated as a beam element.

$$l_u(x) = f_u(x,z)\big|_{z=b_f} = \mu_k(x)\left(d_a + d_b\right) \tag{4}$$

$$\phi_u(x) = \left.\frac{\partial f_u(x,z)}{\partial z}\right|_{z=b_f} = \mu_k(x)\left(\frac{d_a}{b_f} + \frac{d_b\pi}{2b_f}\right) \tag{5}$$

When rigid plates are placed at both ends of the channel member and a compressive force is applied via metal-to-metal contact, such as in a stub column test, three types of buckling displacements along the longitudinal direction have been observed in previous studies [19] as shown in Figure 5. In Figure 5A, the cross-section near the member end opens outward, whereas in Figure 5C, it closes inward. Figure 5B shows a deformation in which the displacement direction differs at the member ends. When the cross-section near the member end opens outward, as shown in Figure 5A, rotation around the width axis is allowed at both end edges of each plate element. Consequently, during distortional buckling, the lip is deformed such that it moves away from the rigid plates at the top and bottom. In this case, a buckling deformation similar to that of a simply supported condition at both ends is formed along the longitudinal direction. This buckling deformation is expressed by Equation (6A). By contrast, when the cross-section near the member ends closes inward (Figure 5C), rotation around the width direction axis of both end edges of each plate element is allowed. However, when the lip at the top and bottom ends contacts the rigid plates, rotation around the width axis at both end edges of each plate element is restrained, resulting in buckling along the longitudinal direction that resembles a clamped-supported condition. This buckling shape is expressed by Equation (6C). In cases where the displacement direction of the cross-section near the member ends differs, rotation around the width direction axis of one end is allowed, whereas the other end is restrained (Figure 5B). This buckling shape is expressed by Equation (6B). Notably, if inward closing deformation occurs in the cross-section near the member ends but the lip does not contact the rigid plates at both ends, rotation around the width axis at both end edges of each plate element is allowed. Consequently, the buckling deformation along the longitudinal direction can be expressed by the displacement function (6A):

$$\text{Pinned} - \text{Pinned} \quad \mu_k(x) = \sin\frac{m\pi x}{L} \tag{6A}$$

$$\text{Pinned} - \text{Clamped} \quad \mu_k(x) = \sin\frac{(m+1)\pi x}{L} + \frac{m+1}{m}\sin\frac{m\pi x}{L} \tag{6B}$$

$$\text{Clamped} - \text{Clamped} \quad \mu_k(x) = \sin\frac{\pi x}{L}\sin\frac{m\pi x}{L} \tag{6C}$$

In Equation (6), m represents the half-wave number, corresponding to a unit half-wavelength along the member length. The elastic critical distortional buckling strength of the channel members was determined using the energy method. Based on the defined displacement functions, the incremental strain energy for each plate element was derived, as expressed in Equation (7). ΔU_1, ΔU_2, and ΔU_3 represent the incremental strain energies of the web, flange, and lip, respectively. As the deformations of both the flanges and lips are axisymmetric, their incremental strain energies are equal.

$$\Delta U_1 = \frac{D}{2}\int_0^L\int_0^{b_w}\left[\left(\frac{\partial^2 w}{\partial x^2}\right)^2 + \left(\frac{\partial^2 w}{\partial y^2}\right)^2 + 2\nu\frac{\partial^2 w}{\partial x^2}\frac{\partial^2 w}{\partial y^2} + 2(1-\nu)\left(\frac{\partial^2 w}{\partial x \partial y}\right)^2\right]\mathrm{d}y\mathrm{d}x \tag{7A}$$

$$\Delta U_2 = \frac{D}{2}\int_0^L\int_0^{b_f}\left[\left(\frac{\partial^2 f_u}{\partial x^2}\right)^2 + \left(\frac{\partial^2 f_u}{\partial z^2}\right)^2 + 2\nu\frac{\partial^2 f_u}{\partial x^2}\frac{\partial^2 f_u}{\partial z^2} + 2(1-\nu)\left(\frac{\partial^2 f_u}{\partial x \partial z}\right)^2\right]\mathrm{d}z\mathrm{d}x \tag{7B}$$

$$\Delta U_3 = \frac{1}{2}\int_0^L\left[EI_l\left(\frac{\partial^2 l_u}{\partial x^2}\right)^2 + GJ_l\left(\frac{\partial \phi_u}{\partial x}\right)^2\right]\mathrm{d}x \tag{7C}$$

When a compressive force is applied to the channel member, assuming a uniform compressive stress distribution across the cross-section, the incremental work done by the external force on the web, flange, and lip elements—denoted as ΔT_1, ΔT_2, and ΔT_3, respectively—is given in Equation (8):

$$\Delta T_1 = \frac{\sigma_{cr,d}t}{2}\int_0^L\int_0^{b_w}\left(\frac{\partial w}{\partial x}\right)^2\mathrm{d}y\mathrm{d}z \tag{8A}$$

$$\Delta T_2 = \frac{\sigma_{cr,d}t}{2}\int_0^L\int_0^{b_f}\left(\frac{\partial f_u}{\partial x}\right)^2\mathrm{d}x\mathrm{d}z \tag{8B}$$

$$\Delta T_3 = \frac{\sigma_{cr,d}A_l}{2}\int_0^L\left(\frac{\partial l_u}{\partial x}\right)^2\mathrm{d}x \tag{8C}$$

The total strain-energy increment was assumed to equal the total work increment due to external forces, allowing the elastic critical distortional buckling strength to be determined by solving it as an eigenvalue problem. Consequently, the resulting elastic critical buckling strength corresponded to the lowest buckling mode. As shown in Figure 3, the buckling behavior of channel members involves distortional, local, and coupled buckling. Therefore, solving the eigenvalue problem may yield elastic buckling strengths for coupled buckling (Figure 3C) or local buckling (Figure 3D), which were not considered in this study. Additionally, since the employed method is based on the upper-bound theorem, the obtained buckling modes may not be optimal for coupled or local buckling. As a result, the estimated strength could be higher than the true value, leading to potential inaccuracies. To exclude coupled and local buckling, the undetermined coefficients d_a and d_b were related by the following equation, and only the distortional buckling mode was considered:

$$d_b = \left(\frac{b_f}{\alpha b_w}\right)^2 d_a \tag{9}$$

As the flange-to-web width ratio b_f/b_w, increased, the out-of-plane flexural stiffness of the flange plate elements decreased, and the restraining effect of the web on the flange increased. Consequently, the out-of-plane flexural deformation under the clamped supported condition in Equation (1) increased. This effect is represented in Equation (9), with its magnitude adjusted by the coefficient α. Figure 6 illustrates how variations in the elastic critical distortional buckling strength correspond to changes in α. The vertical

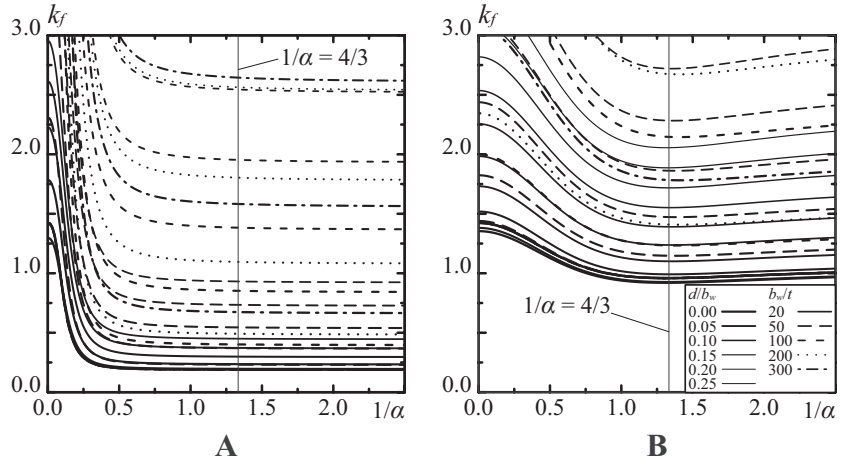

FIGURE 6 | Variations in buckling coefficients for elastic critical distortional buckling. (A) $b_f / b_w = 0.20$. (B) $b_f / b_w = 1.0$.

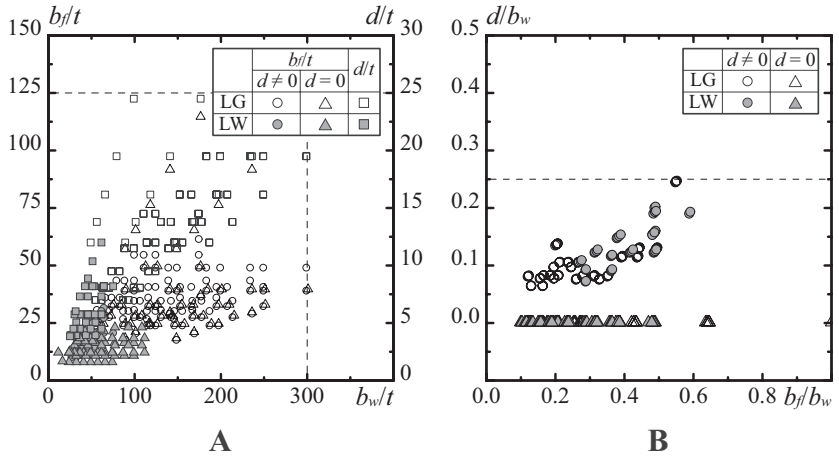

FIGURE 7 | Manufacturing range for the channel and lipped channel members. (A) Range of width-to-thickness ratios. (B) Range of aspect ratios.

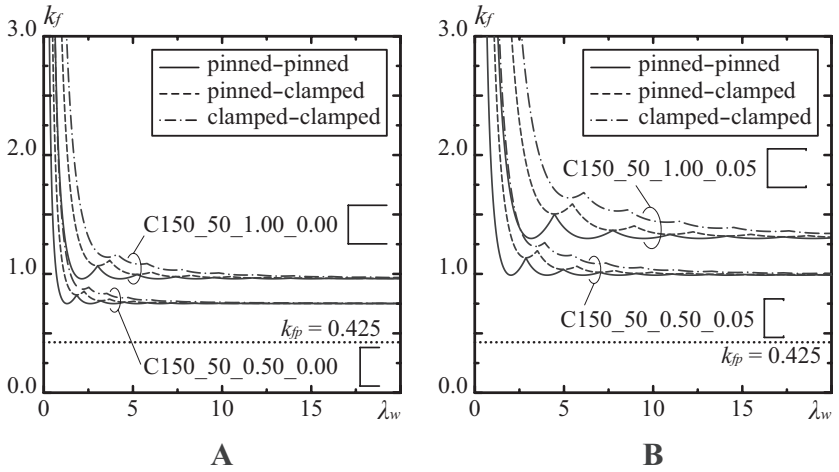

FIGURE 8 | Variation of the flange buckling coefficient, k_f, in response to changes in the web aspect ratio, λ_w. (A) $d/b_w = 0.00$. (B) $d/b_w = 0.10$.

axis represents the elastic critical distortional buckling strength obtained from the numerical analysis results using Equations (7) and (8), converted to the flange buckling coefficient as defined in Table 1, while the horizontal axis represents α. In Figure 6, the web depth b_w is fixed at 150 mm, with the lip-to-web width ratio d/b_w indicated by the line width and the web width-to-thickness ratio b_w/t indicated by the line style. In Figure 6A, where the flange-to-web width ratio b_f/b_w is small, the curve of the flange buckling coefficient does not have a local minimum and converges to a constant value of approximately $\alpha = 1.0$. In Figure 6B, where b_f/b_w is large, the curve of the change in flange buckling coefficient, k_f exhibits a local minimum of approximately $\alpha = 3/4$ regardless of the values of the variables related to cross-sectional geometry. Based on these results, to prevent coupled and local buckling, $\alpha = 3/4$ is adopted as the coefficient that yields the minimum value of the distortional buckling strength, as shown in Figure 3B.

2.2 | Influence of Boundary Condition at Both End Edges on Elastic Critical Distortional Buckling Strength

In this section, the elastic critical distortional buckling strength of the channel member is determined using the energy method, and the scope of the analysis under consideration is described. Figure 7 presents the cross-sectional shape ratios of the domestically manufactured light gauge (LG) [1] and lightweight steel (LW) sections [20]. In Figure 7A, the left vertical axis represents the flange width-to-thickness ratio b_f/t, the right vertical axis represents the lip width-to-thickness ratio d/t, and the horizontal axis represents b_w/t. In Figure 7B, the vertical and horizontal axes represent the lip-to-web width ratio d/b_w and the flange-to-web width ratio b_f/b_w respectively. Lightweight steel sections are indicated by open legends, while light gauge sections are indicated by filled legends. To define the range of domestically manufactured channel members, upper limits were set as follows: $b_w/t \leq 300$, $b_f/t \leq 125$, and $d/t \leq 25$ for the width-to-thickness ratios of the web, flange, and lip, respectively, and $b_f/b_w \leq 1.0$, $d/b_w \leq 0.25$ for the ratios relative to web depth. This defined range represents the primary scope of this study, covering channel member shapes where distortional buckling is not the initial buckling mode. However, only the distortional buckling strength is examined in this study, and comparisons with other buckling modes are reported separately.

Figure 8 depicts the variation of the flange buckling coefficient, k_f, in response to changes in the web aspect ratio λ_w derived based on the energy method described in Section 2.1. The different

boundary conditions at the edges of each plate element are indicated by the line styles. Figure 8A shows a channel member without lips, while Figure 8B illustrates a channel member with lips. To analyze the effect of the buckling half-wavelength, results for both short and long buckling half-wavelengths are presented. The distortional buckling strength is expressed in terms of the flange buckling coefficient, k_f. The dotted line in each graph indicates the buckling coefficient $k_{fp0} = 0.425$ for a plate element that has one free edge and three simply supported edges under a compressive force [21]. Regardless of the presence of lips or the buckling half-wavelength, the displacement function (Equation 6A) produces a sinusoidal half-wave buckling mode (Figure 5A), and is represented by the solid line, resulting in the lowest buckling coefficient across all cross-sectional shapes. Additionally, the flange buckling coefficient decreases with increasing aspect ratio, eventually converging to a constant value unique to each cross-sectional geometry beyond a certain aspect ratio, regardless of the displacement function along the longitudinal direction. By excluding the effects of initial imperfections and material yielding on the buckling behavior, the buckling mode with the lowest critical buckling load is observed. The displacement function along the longitudinal direction that yields the lowest buckling coefficient is given by Equation (6A), which is used for further analysis of the critical elastic distortional buckling strength. The elastic critical distortional buckling strength of a channel member $N_{cr,d,P}$ (Figure 3A,B) is determined using the flange buckling coefficient and gross area A_g, as expressed in Equation (10):

$$N_{cr,d,P} = \min\left(k_{f,pd}, k_{f,d}\right)\frac{\pi^2 E}{12\left(1-\nu^2\right)}\left(\frac{t}{b_f}\right)^2 A_g \tag{10}$$

In Equation (10), $k_{f,pd}$ represents the flange buckling coefficient for pure distortional buckling, as shown in Figure 3A. This coefficient is obtained by setting d_b, the coefficient for clamped-supported buckling mode in Equation (1), to zero, thereby neglecting the out-of-plane flexural deformation of the flange. The flange buckling coefficient $k_{f,pd}$ for pure distortional buckling is given by Equation (11):

$$k_{f,pd} = \frac{\frac{3b_w}{4\pi^2 b_f}\left(\frac{m}{\lambda_w}+\frac{\lambda_w}{m}\right)^2+\left(\frac{mb_f}{\lambda_w b_w}\right)^2\left(1+\frac{12\left(1-\nu^2\right)d^3}{t^2 b_f}\right)+0.425\left(1+\frac{d}{b_f}\right)}{1+\frac{3}{4\pi^2}\left(\frac{b_w}{b_f}\right)^2+\frac{3d}{b_f}}\left(m=1,2,\cdots\right) \tag{11}$$

In Equation (10), $k_{f,d}$ represents the flange buckling coefficient for distortional buckling, as shown in Figure 3B. By considering the out-of-plane flexural deformation of the flange using Equation (9), $k_{f,d}$ can be expressed by Equations (12) and (13):

$$k_{f,d} = \frac{4b_f\left(m_{a1}+m_{a2}+m_{a3}+m_{a4}+m_{a5}\right)}{\pi^2 b_w\left(m_{b1}+m_{b2}+m_{b3}\right)} \tag{12}$$

$$m_{a1} = \frac{b_w}{4b_f}\left(\frac{m}{\lambda_w}+\frac{\lambda_w}{m}\right)^2 \quad \left(m=1,2,\cdots\right) \tag{13A}$$

$$m_{a2} = \left(\frac{m\pi b_f}{\lambda_w b_w}\right)^2\left\{\frac{1}{3}+\left(\frac{3b_f}{4\pi b_w}\right)^2\left[\pi^2-4\pi+8+\frac{3\pi^2-8\pi}{2}\left(\frac{3b_f}{4b_w}\right)^2\right]\right\}\left(m=1,2,\cdots\right) \tag{13B}$$

$$m_{a3} = \left(\frac{3b_f}{4b_w}\right)^2\left\{\frac{1}{2}\left(\frac{3\pi\lambda_w}{16m}\right)^2-\nu\left[\pi-2-\frac{\pi^2-4\pi}{4}\left(\frac{3b_f}{4b_w}\right)^2\right]\right\}\left(m=1,2,\cdots\right) \tag{13C}$$

$$m_{a4} = 4\left(1-\nu^2\right)\frac{b_f d}{t^2}\left(\frac{m\pi d}{\lambda_w b_w}\right)^2\left\{1+\left(\frac{3b_f}{4b_w}\right)^2\left[2+\left(\frac{3b_f}{4b_w}\right)^2\right]\right\}\left(m=1,2,\cdots\right) \tag{13D}$$

$$m_{a5} = 2(1-\nu)\left\{1+\frac{d}{b_f}+\left(\frac{3b_f}{4b_w}\right)^2\left[2+\frac{\pi d}{b_f}+\frac{1}{8}\left(1+\frac{2d}{b_f}\right)\left(\frac{3b_f}{4b_w}\right)^2\right]\right\}\left(m=1,2,\cdots\right) \tag{13E}$$

$$m_{b1} = \left(\frac{b_w}{\pi b_f}\right)^2 \tag{13F}$$

$$m_{b2} = \frac{4b_f}{b_w}\left\{\frac{1}{3}+\left(\frac{3b_f}{4\pi b_w}\right)^2\left[\pi^2-4\pi+8+\frac{3\pi^2-8}{2}\left(\frac{3b_f}{4b_w}\right)^2\right]\right\} \tag{13G}$$

$$m_{b3} = \frac{4d}{b_w}\left\{1+\left(\frac{3b_f}{4b_w}\right)^2\left[2+\left(\frac{3b_f}{4b_w}\right)^2\right]\right\} \tag{13H}$$

In Equation (10), the elastic critical distortional buckling strength $N_{cr,d,P}$, is defined as the strength determined by the lowest value between the flange buckling coefficients $k_{f,pd}$ and $k_{f,d}$, calculated for each buckling half-wavenumber m. Notably, the expression of the flange buckling coefficient, $k_{f,pd}$, for pure distortional buckling is simple compared with the flange buckling coefficient, $k_{f,d}$, for distortional buckling, as it is obtained by setting the coefficient, d_b (applied to the clamped-supported buckling mode in Equation (1)) to zero, thus neglecting the out-of-plane flexural deformation of the flange.

3 | Relationship Between the Geometry of Channel Members and Elastic Critical Distortional Buckling Strength

The relationship between the cross-sectional geometry of the channel member and buckling strength is clarified using the proposed evaluation formula for the elastic critical distortional buckling strength (Equation 10). In this numerical analysis, the web depth b_w, is fixed at 150 mm. Figure 9 illustrates the effect of the lip-to-web width ratio d/b_w on the flange buckling coefficient k_f. The dotted line represents the minimum buckling coefficient of the plate element with one free edge and three simply supported edges, $k_{fp0} = 0.425$. Figure 9A,B differ in terms of flange-to-web width ratio b_f/b_w.

As d/b_w increases, k_f also increases, indicating that a higher d/b_w enhances the distortional buckling strength. When comparing k_{fp0}, with the numerical analysis results (Figure 9A), it is found that in cases where $b_f/b_w = 0.20$ and $d/b_w \leq 0.10$, k_f falls below the minimum buckling coefficient $k_{fp0} = 0.425$. This suggests that, in such cases, the applied stress does not reach the buckling stress required for flange buckling. This phenomenon is further examined by converting k_f to the web buckling coefficient k_w, as shown in Figure 10. The dotted lines represent the buckling coefficient $k_w = 4.0$ for a plate element with simply supported edges, and $k_w = 6.98$ for a plate element with clamped supported edges. In Figure 10A, where the k_f is below $k_{fp0} = 0.425$ in Figure 9A, k_w exceeds 4.0, which is the buckling coefficient for a plate element with simply supported edges. This result indicates that the distortional buckling strength is determined by the local buckling of the web rather than flange buckling. The buckling mode that occurred in this case is shown in Figure 15. Additionally, when k_f exceeds 0.425 and k_w exceeds 4.0, both the flange and web buckle simultaneously. Notably, comparing Figures 9B and 10B, k_f exceeds 0.425, whereas k_w falls below 4.0. In this case, only the flange reaches the buckling condition; therefore, flange buckling determines the distortional buckling strength.

The effect of the flange-to-web width ratio b_f/b_w on k_f is shown in Figure 11. Figure 11A shows a channel member without lips, while Figure 11B shows a channel member with lips. Notably, k_f increased with increasing flange width ratio, with the increase being more significant for channel members with lips. This is likely owing to the addition of the lips, which enhance the restraining effect between each plate element, suppressing flange and web buckling.

Figure 12 shows the effect of b_w/t on k_f. In the channel member without lips (Figure 12A), k_f remained unchanged with variations in b_w/t. This phenomenon occurs because, with a constant plate thickness in the cross-section, ΔU_1 and ΔU_2 in Equation (7), and ΔT_1 and ΔT_2 in Equation (8), change proportionally. By contrast, for the channel member with lips shown in Figure 12B, k_f increased with increasing b_w/t. This is

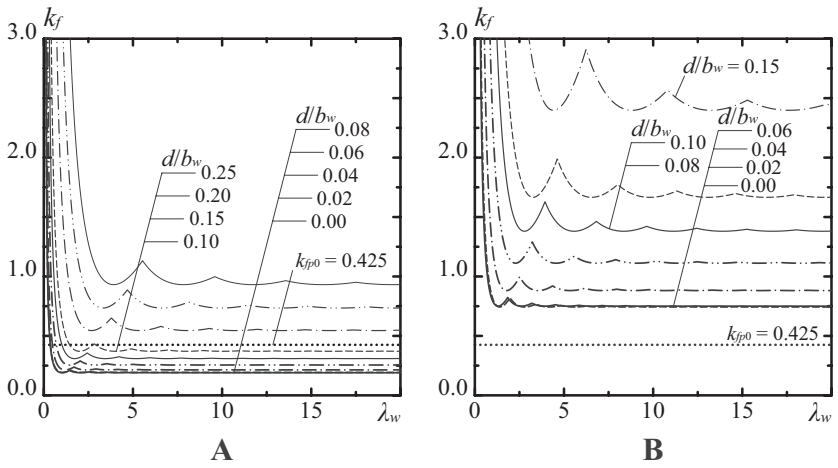

FIGURE 9 | Variation in flange buckling coefficient k_f, with respect to lip-to-web ratio d/b_w. (A) $b_f/b_w = 0.20$, $b_w/t = 50$. (B) $b_f/b_w = 0.50$, $b_w/t = 50$.

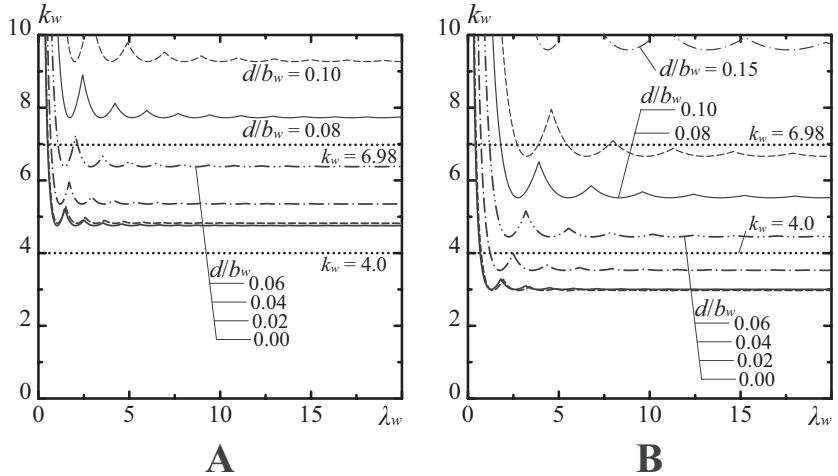

FIGURE 10 | Variation in web buckling coefficient k_w, with respect to lip-to-web ratio d/b_w. (A) $b_f/b_w = 0.20$, $b_w/t = 50$. (B) $b_f/b_w = 0.50$, $b_w/t = 50$.

attributed to the decrease in ratio of the flange's out-of-plane flexural stiffness to the lips' in-plane stiffness, as the b_w / t increases while the lip width remains constant. Consequently, the restraining effect of the lip on the flange increases, resulting in an increase in k_f.

The results obtained in this section are summarized in Figure 13. The principle that the minimum buckling coefficient at a given buckling half-wavenumber, m, coincides with the converged value of the buckling coefficient being utilized. Numerical calculations were conducted by setting $m = 1$ to determine the minimum buckling coefficient. The vertical axis represents the lip-to-web width ratio d / b_w, whereas the horizontal axis represents the flange-to-web width ratio b_f / b_w. The coefficient b_w / t is indicated by different line types. The line type without symbols represents the boundary, where $k_f / k_{fp} = 1.0$. The line type with circles denotes the boundary where $k_w = 4.0$, whereas the line type with squares represents the boundary where $k_w = 6.98$. The coefficient k_{fp} is the buckling coefficient of a plate element with one free edge and three simply supported edges, considering the influence of the buckling half-wavelength. It is calculated using Equation (14):

$$k_{fp} = 0.425 + \left(\frac{m_{cr} b_f}{\lambda_w b_w} \right)^2 \tag{14}$$

The parameter m_{cr} represents the buckling half-wavenumber that minimizes the elastic critical distortional buckling strengths $N_{cr,d,P}$. The converged value of Equation (14) matches the minimum buckling coefficient k_{fp0} for a plate element with one free edge and three simply supported edges. The line marked with triangles marks the boundary between regions where distortional buckling strength is determined by pure distortional (Figure 3A) and distortional buckling (Figure 3B). Figure 14, which extracts results for a web width-to-thickness ratio $b_w / t = 50$ from Figure 13, serves as a representative example to clarify Figure 13. The regions separated by the boundary lines for each buckling coefficient are labeled as A, B, C, D, and E.

Regions A and B correspond to areas where k_w exceeds 6.98. This region was significantly influenced by the web width-to-thickness ratio and expanded with an increase in this ratio. It is known that in cases where the stress within the plate element is

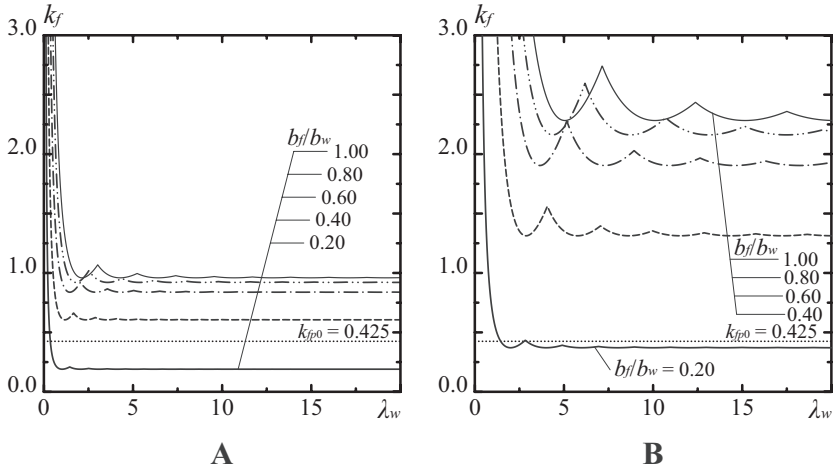

FIGURE 11 | Variation in flange buckling coefficient k_f, with respect to flange-to-web ratio d / b_w. (A) $d / b_w = 0.00$, $b_w / t = 50$. (B) $d / b_w = 0.10$, $b_w / t = 50$.

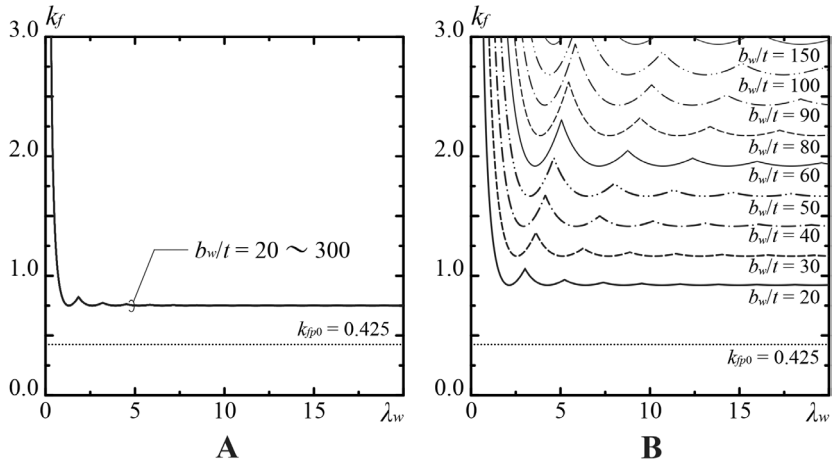

FIGURE 12 | Variation in flange buckling coefficient k_f, with respect to flange-to-web ratio d / b_w. (A) $b_f / b_w = 0.50$, $d / b_w = 0.00$. (B) $b_f / b_w = 0.50$, $d / b_w = 0.10$.

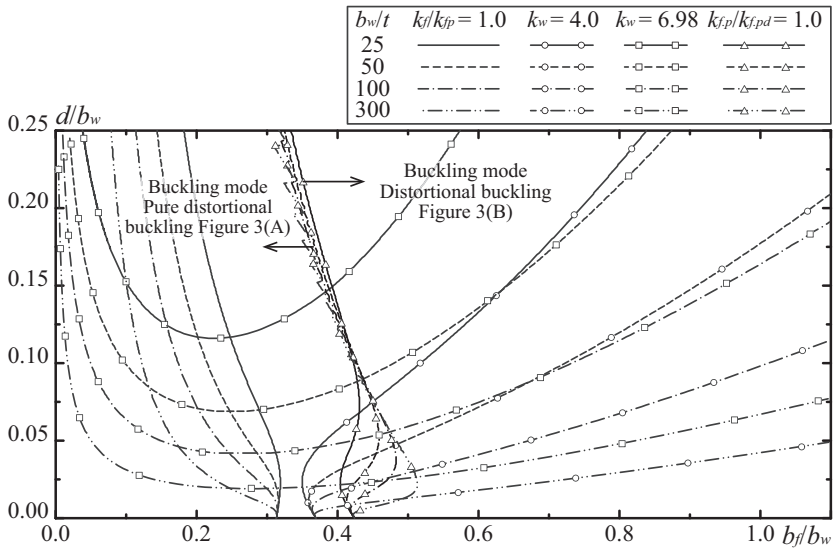

FIGURE 13 | Changes in buckling coefficients of flange and web with respect to the cross-sectional geometry.

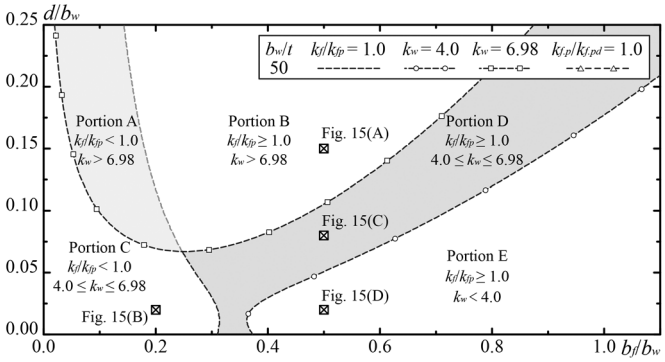

FIGURE 14 | Boundary lines of distortional buckling modes ($b_w / t = 50$).

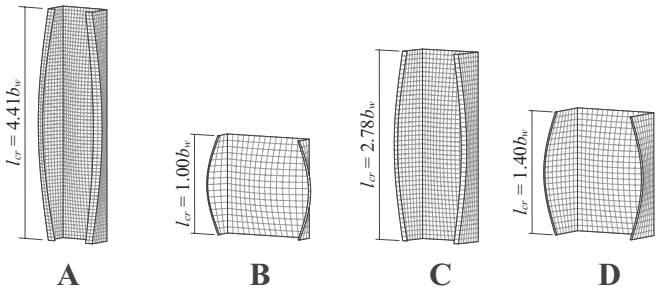

FIGURE 15 | Distortional buckling modes are shown in Figure 14. (A) Regions A and B, (B) Region C, (C) Region D, (D) Region E.

uniform, such as in pure compression, the buckling coefficient of that plate element does not exceed 6.98 [21]. As this study focuses only on distortional buckling and disregards local and coupled buckling, as shown in Figure 3, buckling modes with $k_w \geq 6.98$, as shown in Figure 10, can be examined. However, in practice, the buckling coefficients cannot exceed 6.98, and the critical buckling strength is determined by primary modes other than the distortional buckling mode. In other words, Regions A and B, where the buckling coefficient exceeded 6.98, were the areas in which distortional buckling did not occur. The buckling mode with a half-wavelength occurring in these regions is illustrated in Figure 15A. where l_{cr} denotes the buckling half-wavelength. Notably, Regions A and B are delineated by the boundary line where $k_f / k_{fp} = 1.0$, as these regions involve different buckling modes. However, because no buckling mode with a coefficient exceeding 6.98 exists in plate elements subjected to a uniform compressive force, no further examination was conducted in this study. Region C is defined as the area where $k_f / k_{fp} < 1.0$ and the web buckling coefficient is in the range $4.0 \leq k_w \leq 6.98$. Based on the buckling coefficients, it can be concluded that distortional buckling initiated by the local buckling of the web occurs in this region. The buckling mode corresponds to that shown in Figure 15B, with a buckling half-wavelength l_{cr} of 1.00 b_w, reflecting the characteristics of local buckling under simply supported

TABLE 2 | Classification of distortional buckling behaviors.

Regions	Figure 15	k_w	k_f / k_{fp}	Buckling mode
A, B	(A)	$k_w > 6.98$	—	Distortional buckling does not occur
C	(B)	$4.0 \le k_w \le 6.98$	$k_f / k_{fp} < 1.0$	Distortional buckling initiated by local buckling of the web
D	(C)	$4.0 \le k_w \le 6.98$	$k_f / k_{fp} \ge 1.0$	Simultaneous buckling of the flange (including the lip) and the web
E	(D)	$k_w < 4.0$	$k_f / k_{fp} \ge 1.0$	Distortional buckling is initiated by buckling of the flange including the lip

conditions. Notably, when the buckling strength is determined by the local buckling of the web, each plate element comprising the cross-section exerts mutual restraint effects. Consequently, both the flange and web deform, resulting in the overall member exhibiting distortional buckling behavior, where the flange and lip junction lines either opening outward or closing inward (Figure 15B). Region D is characterized by a flange buckling coefficient ratio, $k_f / k_{fp} \ge 1.0$ and a web buckling coefficient in the range $4.0 \le k_w \le 6.98$, indicating simultaneous buckling of the flange (including the lip) and the web. The corresponding buckling modes are shown in Figure 15C. Additionally, Region D is significantly influenced by the web width-to-thickness ratio; as this ratio increases, Region D decreases, as illustrated in Figure 13. Region E represents the area where $k_f / k_{fp} \ge 1.0$ and the $k_w < 4.0$, indicating that the distortional buckling strength is determined by the buckling of the flange, including the lip. The distortional buckling mode in this case corresponded to that shown in Figure 15D. As shown in Figure 13, Region E shrinks with an increase in the web width-to-thickness ratio. Table 2 summarizes the definitions of these regions. As shown in Figure 15 and Table 2, when based solely on the buckling modes, the regions were considered as having the same distortional buckling behavior. However, analysis using the buckling coefficients revealed that the four buckling modes represented distinct phenomena. Additionally, the lip-to-web width and web width-to-thickness ratios exerted a dominant influence on the boundary lines between these buckling mode regions.

The boundary line distinguishing pure distortional buckling from distortional buckling, represented by the line pattern with triangle markers in Figure 13, separates Regions B, D, and E, enabling a more precise classification of distortional buckling behavior within these areas. However, further categorization was not pursued to avoid complicating the discussions. Notably, the boundary line for the pure distortional and distortional buckling modes transitions within the b_f / b_w range of 0.3–0.5, indicating that pure distortional buckling occurs within a narrower flange width ratio.

4 | Design Equation of Elastic Critical Distortional Buckling and Comparison With Existing Design Formula

4.1 | Proposed Design Equation for Elastic Critical Distortional Buckling

In Chapter 2, the elastic critical distortional buckling strength formula is proposed to account for variations in member length. When the displacement function (Equation 6A), which allows rotation along the width direction of the edge plate element, is used as the longitudinal displacement function, the minimum buckling coefficient obtained at a specific buckling half-wave number m aligns with the convergence value of the buckling coefficient obtained when the member length is sufficiently long. This finding suggests that evaluating the elastic critical distortional buckling strength based on the minimum buckling coefficient for a given half-wavelength m can conservatively establish a design equation for the distortional buckling strength. Thus, the proposed formula, Equation (10), is simplified to enable an approximate evaluation of the elastic critical distortional buckling strength as it varies with cross-sectional geometry. When comparing the flange buckling coefficient $k_{f,pd}$ for pure distortional buckling (Figure 3A (Equation 11) with the flange buckling coefficient $k_{f,d}$ for distortional buckling (Figure 3B (Equations 12 and 13), it was observed that the $k_{f,pd}$, which excludes out-of-plane flexural deformation of the flange, provides a simpler expression for pure distortion buckling. Therefore, in this study, the buckling strength obtained using the flange buckling coefficient $k_{f,pd}$ for pure distortional buckling, is considered as the reference distortional buckling strength. The buckling strength is then adjusted by a factor that varies with the cross-sectional geometry of the channel member based on the flange buckling coefficient $k_{f,pd}$, The elastic critical distortional buckling strength of the channel member is approximately evaluated by multiplying the reference distortional buckling strength by the geometry-dependent factor. The flange buckling coefficient for the minimum buckling strength at a certain buckling half-wave number, m, is determined by setting $m = 1$ in Equation (11) and partially differentiating with respect to the web aspect ratio, λ_w. Consequently, the stationary point is identified, and the web aspect ratio, $\lambda_{w,cr}$, that minimizes the distortional buckling coefficient is derived, as shown in Equation (15):

$$\lambda_{w,cr} = \sqrt[4]{1 + \frac{4\pi^2}{3}\left(\frac{b_f}{b_w}\right)^3\left(1 + \frac{12(1-\nu^2)d^3}{t^2 b_f}\right)} \tag{15}$$

By using $\lambda_{w,cr}$, the flange buckling coefficient, $k_{f,pd}$, that determines the reference distortional buckling strength can be expressed, as shown in Equation (16):

$$k'_{f,pd} = \frac{\frac{3b_w}{4\pi^2 b_f}\left(\frac{1}{\lambda_{w,cr}} + \lambda_{w,cr}\right)^2 + \left(\frac{b_f}{\lambda_{w,cr} b_w}\right)^2\left(1 + \frac{12(1-\nu^2)d^3}{t^2 b_f}\right) + 0.425\left(1 + \frac{d}{b_f}\right)}{1 + \frac{3}{4\pi^2}\left(\frac{b_w}{b_f}\right)^2 + \frac{3d}{b_f}} \tag{16}$$

Subsequently, a factor for evaluating the variation in the distortional buckling strength according to the cross-sectional geometry of the channel member was determined. Figure 16A illustrates the variation in the distortional buckling coefficient ratio, $k_{f,d}/k'_{f,pd}$, with respect to the change in lip-to-web width ratio, d/b_w, for each flange-to-web width ratio, b_f/b_w. The results indicate that the distortional buckling coefficient ratio varies approximately linearly with the change in the lip-to-web width ratio and is determined by the intercept and slope corresponding to the flange-to-web width ratio, with little influence from the web width-to-thickness ratio b_w/t. As shown in Figure 16A, the effect of the web width-to-thickness ratio on the distortional buckling coefficient ratio was negligible. The intercept and slope for each flange width ratio are denoted as β and γ, respectively, when the web width-to-thickness ratio is set to $b_w/t = 300$, and the variations in β and γ with respect to the flange-to-web width ratio are shown in Figure 16B. The legend marked by circles indicates the variation of β, and the legend marked by squares represents the variation of γ. In this study, the variations in β and γ are approximated by simple linear equations, as shown in Equations (17) and (18):

$$\beta = \min\left(1.0, -\frac{b_f}{6b_w} + \frac{16}{15}\right) \tag{17}$$

$$\gamma = \min\left(0.0, -\frac{3b_f}{10b_w} + 0.06\right) \tag{18}$$

Using Equations (15–18), the design equation for the elastic critical distortional buckling strength, $N_{cr,d,\mathrm{Design}}$, of the channel member can be determined using the approximate flange buckling coefficient, $k_{f,d,\mathrm{Design}}$, as shown in Equation (20) and given by Equation (19):

$$N_{cr,d,\mathrm{Design}} = k_{f,d,\mathrm{Design}} \frac{\pi^2 E}{12(1-\nu^2)} \left(\frac{t}{b_f}\right)^2 A_g \tag{19}$$

$$k_{f,d,\mathrm{Design}} = \left(\gamma \frac{d}{b_w} + \beta\right) k'_{f,pd} \tag{20}$$

4.2 | Validation of Proposed Elastic Critical Distortional Buckling Strength Formula and Design Equation

To validate the proposed elastic critical distortional buckling strength formula (Equation 10) and design equation (Equation 19), comparisons were made against eigenvalue analysis results obtained using FEM. Additionally, the proposed design equation was compared with the elastic distortional buckling strength equations proposed by Hancock and Schafer, hereafter referred to as the Hancock and Schafer models, respectively. Eigenvalue analysis was conducted using the general-purpose FEM software MSC Marc 2019 [22]. Cross-sectional geometry was set as the analysis parameter, and an overview of the analytical model is presented in Figure 17. The analysis model consisted of four-node shell elements with a 4 mm square mesh, determined based on a convergence study. The ends of the analysis model were connected to centroid positions (A and B) using rigid elements. The rotations at points A and B were restrained, whereas displacement along the x-axis at point B was permitted. Additionally, the z-axis displacement along the web-flange junction lines was restrained to prevent global buckling modes by applying appropriate boundary conditions. An external vertical load P, was applied at point B. The material properties were set with a Young's modulus, E, of 205 000 N/mm^2 and a Poisson's ratio, ν, of 0.3. For the analysis variables, the web depth, b_w, was fixed at 150 mm, and the web aspect ratio, λ_w, was fixed at 100. Based on Figure 7, the flange-to-web width ratio, b_f/b_w, was varied from 0.1 to 1.0, and the lip-to-web width ratio, d/b_w, was varied from 0.0 to 0.25. In this range, the analysis cases included cases where the first buckling modes corresponded to the distortional buckling modes (Figure 3A,B) and cases where the buckling mode was classified as coupled and local buckling (Figure 3C,D). As this study focused on distortional buckling, only the results where the first buckling mode corresponding to distortional buckling were extracted, in accordance with the buckling mode classifications shown in Figure 3.

A comparison with the eigenvalue analysis results obtained using FEM is shown in Figures 18 and 19. In Figure 18A, the vertical axis represents the ratio of the flange buckling

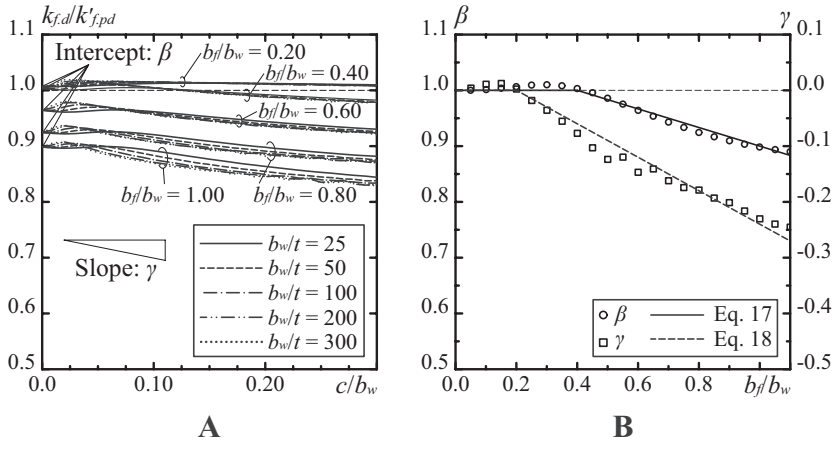

FIGURE 16 | Distortional buckling modes are shown in Figure 14. (A) Regions A and B, (B) Region C, (D) Region D, (D) Region E.

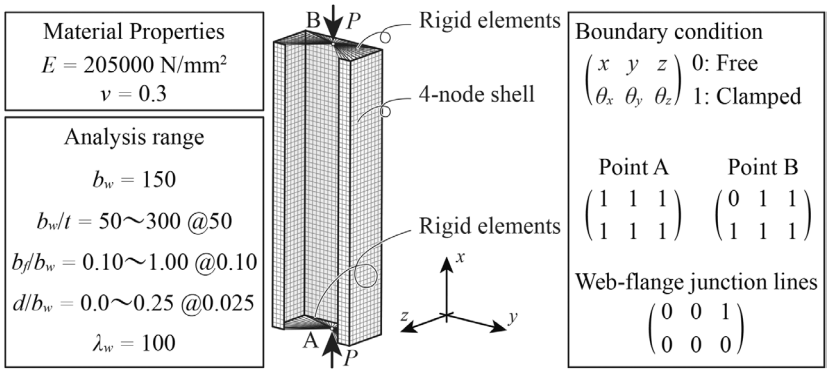

FIGURE 17 | Overview of the finite element analysis model.

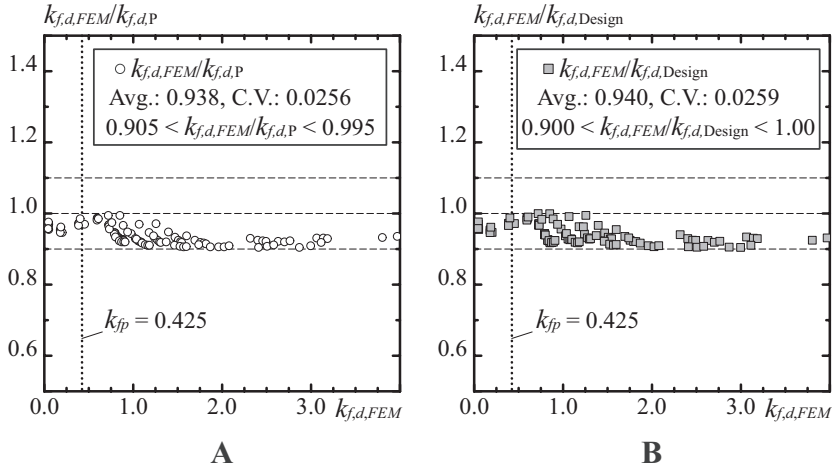

FIGURE 18 | Comparison with FEM results. (A) Evaluation formula. (B) Proposed design equation.

coefficient $k_{f,d,FEM}$, derived from the eigenvalue analysis results to the flange buckling coefficient $k_{f,d,P}$, obtained using the proposed evaluation formula (Equation 10). Similarly, in Figure 18B, the vertical axis shows the ratio of $k_{f,d,FEM}$ to the flange buckling coefficient, $k_{f,d,Design}$, calculated using the simplified design equation (Equation 19). In Figure 19A,B, the vertical axis shows the ratios of $k_{f,d,FEM}$ to $k_{f,d,Hancock}$ and $k_{f,d,Schafer}$, respectively, where $k_{f,d,Hancock}$ and $k_{f,d,Schafer}$ are the flange-buckling coefficients derived from the Hancock and Schafer models. The vertical dotted line in the figures indicates the minimum buckling coefficient of 0.425 for a plate element with one free edge and three simply supported edges. The eigenvalue analysis results with $k_{f,d,FEM} < 0.425$ correspond to Region C, where distortional buckling is initiated from the local buckling of the web.

A comparison of the proposed evaluation formula shown by the circle legend in Figure 18A, with the eigenvalue analysis results revealed that the average of the FEM eigenvalue analysis results for the proposed evaluation formula was 0.938 with a coefficient of variation of 0.00256. This indicates that the proposed evaluation formula provides an accurate assessment of the elastic critical distortional buckling strength of channel members. In Figure 18B, the average of the FEM eigenvalue analysis results for the simplified design equation (Equation 19) was 0.940, with a coefficient of variation of 0.00259. This demonstrates that the simplified design equation evaluates the elastic critical distortional buckling strength with an accuracy similar to that of the proposed formula. However, both the proposed formula and simplified design equation yielded slightly unconservative assessments, with an error range of 0%–10% compared with the eigenvalue analysis results. This is because the proposed method is based on the upper-bound theorem. In practical members, factors such as initial imperfections and eccentricities can reduce the buckling strength, potentially leading to a lower buckling strength than that indicated by the eigenvalue analysis results. Therefore, applying a safety factor of at least 10% to the elastic distortional buckling strength obtained from the proposed evaluation formula and simplified design equation is recommended.

Subsequently, the Hancock and Schafer models were compared with the eigenvalue analysis results. Notably, the application range of the Hancock equation was $0.4 \leq b_f / b_w$; thus, analysis cases outside this range were also included in Figure 19A. Cases outside the application range ($b_f / b_w < 0.4$) were shown with an open marker, while cases within the range ($b_f / b_w \geq 0.4$) were indicated with a filled marker. However, the Schafer model did not specify an appropriate range. Compared with the proposed method, substantial variability was observed when comparing the eigenvalue analysis results with that of the Hancock and Schafer models. Specifically, a significant variation was observed near a buckling coefficient of 0.425 (indicated by the

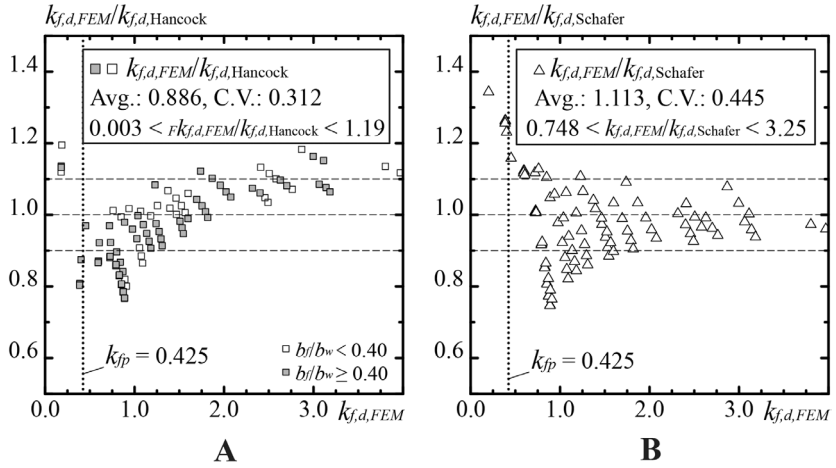

FIGURE 19 | Comparison with FEM results. (A) Hancock model [3]. (B) Schafer model [8].

vertical dotted line). The distortional buckling mode that arises in this buckling coefficient range corresponds to the distortional buckling initiated by the local buckling of the web (denoted as Region C). Therefore, the Hancock and Schafer models, which model only the flange and lip (as illustrated in Figure 2), did not accurately evaluate the elastic critical distortional buckling strength initiated by the local buckling of the web. Furthermore, discrepancies in the evaluation results for the distortional buckling strength were evident even in regions with higher buckling coefficients beyond the range of 0.425. This variability arises from the limitations of representing the restraining effect of the web on the flange with elastic springs, which inadequately represent the interactions among the plate elements.

Overall, the proposed evaluation formula (Equation 10) and the design equation (Equation 19), which utilize a mechanical model representing the entire cross-section, are applicable even in cases where distortional buckling strength is initiated by local buckling of the web—a condition that existing flange-based equations cannot assess. The proposed methods enable the continuous and precise evaluation of distortional buckling initiated by the local buckling of the web, as well as other distortional buckling forms that occur in channel-section members. The design formula proposed in this study was validated through eigenvalue analysis using FEM; however, it has not yet been compared with results from structural experiments. In future work, comparisons with experimental data will be conducted to further verify its effectiveness.

5 | Conclusion

This study investigates the effects of various geometric parameters of channel members on the elastic critical distortional buckling strength using an energy method. The main findings are summarized below:

1. A mechanical model was proposed to represent the distortional buckling of channel and lipped channel members—regarded as flange buckling in previous studies—by expressing the buckling waveforms of the web, flange, and lip as a series of functions. Based on this model, an evaluation formula for critical elastic distortional buckling strength was derived. Additionally, a simplified design equation was developed.
2. Three types of displacement functions along the longitudinal direction were defined based on the differences in the cross-sectional deformation directions near the ends of the member. The elastic critical distortional buckling strength decreased with increasing aspect ratio, regardless of the displacement function along the longitudinal direction. Beyond a certain aspect ratio, it converged to a constant value unique to each cross-sectional geometry.
3. Distortional buckling was categorized into four modes based on the buckling coefficient, with the boundary lines between each region primarily influenced by the web width-to-thickness and lip-to-web width ratios.
   i. Regions A and B represented areas where the web buckling coefficient exceeded the buckling coefficient of 6.98, and first buckling modes other than distortional buckling were present.
   ii. Region C was defined by a flange buckling coefficient ratio below 1.0, leading to distortional buckling initiated by the local buckling of the web.
   iii. Region D was characterized by a web buckling coefficient above the buckling coefficient of 4.0 (for a plate with simply supported edges), and the flange buckling coefficient ratio was above 1.0, resulting in the simultaneous buckling of the web and flange as distortional buckling occurred.
   iv. Region E represented the area where the web buckling coefficient fell below 4.0, which is the smallest value for the buckling of a plate with simply supported edges, and where distortional buckling originated from flange buckling.
4. The evaluation formula for the distortional buckling strength proposed by Hancock and Schafer, which interpreted distortional buckling as flange buckling, showed variability and cannot accurately evaluate the elastic critical distortional buckling strength, particularly when local web buckling initiated the distortional buckling. Additionally, even within the applicable range of the proposed formula, the variability remained high owing to the inadequate substitution of the restraining effect of the web

on the flanges with elastic springs, leading to an inaccurate evaluation of the distortional buckling strength.

5. The proposed evaluation formula (Equation 10) and simplified design equation (Equation 19) enabled the precise determination of the elastic critical distortional buckling strength, even for the range where distortional buckling occurs by initiating local buckling of the web, which cannot be addressed by the evaluation formulae in previous studies. These proposed methods allowed for the continuous evaluation of a series of distortional buckling occurrences in channel members.

Acknowledgments

This work was supported by JSPS KAKENHI (grant number JP20H02294).

Conflicts of Interest

The authors declare no conflicts of interest.

Data Availability Statement

All information and data are given in the text completely.

References

1. *Guide for Designing Cold-Formed Steel Structures*, 2nd ed. (Gihodo Shuppan Co. Ltd, 2014). (in Japanese).

2. American Iron and Steel Institute (AISI), *North American Specification for the Design of Cold-Formed Steel Structural Members* (American Iron and Steel Institute, 2020).

3. S. C. W. Lau and G. J. Hancock, "Distortional Buckling Formulas for Channel Columns," *Journal of Structural Engineering* 113, no. 5 (1987): 1063–1078, https://doi.org/10.1061/(ASCE)0733-9445(1987)113:5(1063).

4. G. J. Hancock, "Design for Distortional Buckling of Flexural Members," *Thin-Walled Structures* 27, no. 1 (1997): 3–12, https://doi.org/10.1016/0263-8231(96)00020-1.

5. G. J. Hancock, C. A. Rogers, and R. M. Schuster, "Comparison of the Distortional Buckling Method for Flexural Members With Tests," *Proceeding 13th International Specialty Conference on Cold-Formed Steel Structures* (1996), 125–138.

6. G. J. Hancock, Y. B. Kwon, and E. S. Bernard, "Strength Design Curves for Thin-Walled Sections Undergoing Distortional Buckling," *Journal of Constructional Steel Research* 31, no. 2–3 (1994): 169–186, https://doi.org/10.1016/0143-974X(94)90009-4.

7. B. W. Schafer and T. Peköz, "Laterally Braced Cold-Formed Steel Flexural Members With Edge Stiffened Flanges," *Journal of Structural Engineering* 125, no. 2 (1992): 118–127, https://doi.org/10.1061/(ASCE)0733-9445(1999)125:2(118).

8. B. W. Schafer, "Local, Distortional, and Euler Buckling of Thin-Walled Columns," *Journal of Structural Engineering* 128, no. 3 (2022): 289–299, https://doi.org/10.1061/(ASCE)0733-9445(2002)128:3(289).

9. B. W. Schafer, *Distortional Buckling of Cold-Formed Steel Columns* (Final Report Sponsored by the American Iron and Steel Institute, 2000).

10. B. W. Schafer and T. Peköz, "Direct Strength Prediction of Cold-Formed Steel Members Using Numerical Elastic Buckling Solutions," *Proceeding 14th International Specialty Conference on Cold-Formed Steel Structures* 4 (1998): 69–76.

11. G. Winter, "Thin-Walled Structures Theoretical Solutions and Test Results," *IABSE Preliminary Publication of the 8th Congress* (1968), 101–112.

12. R. D. Ziemian, *Guide to Stability Design Criteria for Metal Structures*, 6th ed. (John Wiley, 2010).

13. American Iron and Steel Institute (AISI), *AISI Specification for the Design of Cold-Formed Steel Structural Members* (American Iron and Steel Institute, 1996).

14. I. Iwamoto, M. Kimura, and T. Ogawa, "Study on Lip Stiffening Effect of Thin Plate Elements," *Journal of Structural and Construction Engineering (Transactions of AIJ)* 548 (2001): 147–151. (in Japanese), https://doi.org/10.3130/aijs.66.153_3.

15. K. Mitsui and K. Ikarashi, "Buckling Strength and Behavior of Elastic Local Buckling for Cold-Formed Channel Members Under Compression," *Journal of Structural and Construction Engineering (Transactions of AIJ)* 56, no. 790 (2021): 1685–1692. (in Japanese), https://doi.org/10.3130/aijs.86.1685.

16. K. Mitsui and K. Ikarashi, "Elastic Critical Local Buckling Load and Behavior of Local Buckling for Cold-Formed Lipped Channel Steel Member Under Compression," *Japan Architectural Review* 7, no. 1 (2024): 12432, https://doi.org/10.1002/2475-8876.12432.

17. K. Mitsui, K. Ikarashi, T. Kobashi, and R. Kuwada, "Elastic Critical Local Buckling Stress in Cold-Formed Lipped Channel and Hat Sections Under Uniform Compression," *Thin-Walled Structures* 191 (2023): 111064, https://doi.org/10.1016/j.tws.2023.111064.

18. K. Ikarashi and T. Wang, "A Method for Evaluation of Elastic Buckling Strength of H-Shaped Steel Member Under Bending-Shear and Axial Force," *Journal of Structural and Construction Engineering (Transactions of AIJ)* 613 (2007): 137–146. (In Japanese), https://doi.org/10.3130/aijs.72.137_1.

19. K. Mitsui, A. Watanabe, T. Kobashi, and K. Ikarashi, "Effect of Geometrical Imperfection on Analytical Buckling Strength of Cold-Formed Lipped Channel Steel Member Under Compression," *Journal of Structural and Construction Engineering (Transactions of AIJ)* 86, no. 779 (2021): 157–167 (in Japanese), https://doi.org/10.3130/aijs.86.157.

20. Japanese Industrial Standards Committee, *Light Gauge Steel Sections for General Structure* (JIS G 3350, 2017). (in Japanese).

21. Architectural Institute of Japan (AIJ), *AIJ Recommendations for Stability Design of Steel Structures* (Architectural Institute of Japan, 2018). (in Japanese).

22. *Epi Info* [MSC Software Corporation]. Marc Version 2019 Volume A-D (2020).